Encoding of Component and Pattern Motion in Awake Mouse Visual Cortex and Superior Colliculus

Chen Chen

Charlottesville, VA

Bachelor of Science, Tongji University, 2017

A predissertation research project presented to the graduate faculty of the University of Virginia in candidacy for the degree of Master of Arts

Department of Psychology

University of Virginia

December 2022

Committee Members: Prof. Jianhua Cang

Prof. Daniel Meliza

Abstract

The encoding of motion features by the visual system is critical for an animal's survival in a dynamic environment. As one of the important features, the detection of motion direction varies to some degree in different species and brain areas. In mice, orientation (or motion axis) selective cells are consistently reported in the primary visual cortex (V1), whereas a large proportion of cells in the superficial layer of the Superior Colliculus (SC) are direction selective. However, little is known about how exactly these two structures respond to complex motion in awake mice. To address this question, we presented the animals with drifting gratings and moving plaids which are formed by superimposing two sinusoidal gratings. We used two-photon calcium imaging to record neuronal responses in layer II/III of V1 and superficial SC. We found that the majority of V1 neurons are sensitive to two opposite directions of the gratings with a narrow tuning curve, while superficial SC neurons are tuned specifically to a range of directions with a broader curve. Next, we identified a group of V1 neurons sensitive to the component directions of the plaid. These component motion-selective neurons display tuning curves with four peaks, each of which indicates the preferred direction of the elemental drifting grating of plaids. On the contrary, most SC neurons are selective for pattern motion such that they prefer the global direction of the plaid. In general, our results suggest that the mouse V1 is essential for encoding elemental motion whereas the SC is important for global motion, indicating different roles of V1 and SC in processing visual motion.

Keywords: functional imaging; drifting grating; direction selectivity; plaid; pattern motion; component motion, v1, superior colliculus

Introduction

Detecting surrounding movement in a dynamic environment is important for animals' survival (Albright & Stoner, 1995). A fundamental question in visual processing is how motion features are encoded in the visual system, such as direction, shape, speed, and luminance. Many well-designed visual stimuli have been used to study the underlying neuronal mechanism, which has led to a number of computational models (Hildreth & Koch, 1987). Additive plaid stimuli have been used to present a single coherent perception in certain cases, such as superimposing two symmetric crossed moving gratings (Adelson & Movshon, 1982). By using this kind of plaids, two distinct populations have been identified in the cat and primate visual cortex to characterize the stage of visual motion processing for complex motion inputs (Movshon et al., 1985; Albright & Stoner, 1995). The first group of cells, which are sensitive to the moving directions of each elemental grating of plaids ("component motion selective cells"), are mostly found in V1 (Movshon et al., 1985; Gizzi et al., 1990). The other group of cells, on the contrary, have the ability to combine elementary information and respond to the global motion direction of plaids ("pattern motion selective cells"). The pattern cells are mostly found in the higher visual cortex of primates that correspond to visuomotor transformation and integration, such as the middle temporal area (MT) and medial superior temporal area (MST) (Rodman & Albright., 1989; Gizzi et al., 1990; Khawaja at al., 2009).

Due to the availability of genetic, viral, and imaging tools, mice have become a popular research model in recent years. Although mouse V1 is relatively small and lacks orientation columns compared to cats and primates (Hübener, 2003; Ohki et al., 2005; Ohki & Reid, 2007; Bonin et al., 2011), the processing of

complex motion was assumed similar (Movshon et al., 1985; Gizzi et al., 1990). However, the results turned out inconclusive. One study shows that only component motion selective cells but not pattern motion selective cells were found in mouse V1 (Juavinett & Callaway, 2015), while two other studies show that mouse V1 had both component and pattern motion selective cells and they functioned similarly as other species on complex motion (Muir et al., 2015; Palagina et al., 2017). All these studies were performed in the monocular V1 of anesthetized mice. One of the possible reasons for this controversy is that the used plaids stimuli were different, in terms of component gratings, presentation duration, and stimulus size. But it remains unclear whether mouse V1 encodes the global motion or not and what is the motion processing in the awake mouse.

In addition, unlike primates, whose visual information is mostly sent from the retina to the lateral geniculate nucleus (LGN) and further relayed to the V1, the superior colliculus (SC) in mice receives more than 85% of retinal ganglion cell (RGC) inputs (Ellis et al., 2016; Cang et al., 2018). Most direction selective RGCs directly project to the superficial layer of SC (Dhande & Huberman, 2014). About 60 - 70% of visually responsive neurons in the surface of SC are direction-selective (Wang et al., 2010; Inayat et al., 2015) and they inherit the direction selectivity properties from the retina (Shi et al., 2017). Therefore, it is intriguing to know how the SC encodes the complex motion and whether patterns or component cells are responding to plaids. Moreover, the comparison between awake mouse V1 and SC could give us more insights into their roles and functional organizations during motion processing.

Here, we presented sinusoidal gratings and plaids to awake mice and applied two-photon calcium imaging of V1 and SC to record their neuronal responses. When the animals were given drifting gratings, layer II/III cells of V1 are prominently bi-direction selective (axis selective or orientation selective), while most of the superficial SC cells are direction selective. We then determined their tuning curves to plaids and used a partial correlation coefficient between actual and predicted tuning curves to identify component and pattern cells. Interestingly, among bi-direction selective cells in V1, about 11.88 % (12/101) are found to be component selective. For SC, more than half of direction-tuned cells (57.45%; 81/141) show robust pattern motion selectivity. Our results indicate that different mechanisms compute complex motion signals in V1 and SC.

Materials and Methods

Animals. Adult C57BL/6 mice of either sex were used in this study. Wild-type (n=5, 2-6 months old) mice were used for SC imaging, and transgenic VIP (n=2, 2-6 months old) or SST (n=3, 2-6 months old) mice were used for V1 imaging that are expressing the red fluorescent protein tdTomato in VIP or SST neurons. The transgenic mice were obtained by crossing VIP-IRES-cre mice (The Jackson Laboratory, Stock #010908; RRID: IMSR_JAX:010908) or SST-IRES-cre mice (The Jackson Laboratory, Stock #013044; RRID: IMSR_JAX:013044) with an Ai9 line (RCL-tdT, Stock #007909; RRID: IMSR_JAX:007909) in our colony. However, we did not find any obvious difference in coding component motion vs. pattern motion for either VIP or SST cells. All mice were kept on a 12 h light/dark cycle in the animal room. Two to five animals were housed per cage. Whenever possible, the animals were housed with other for keeping their social activity including after surgery. All experimental procedures were approved by the University of Virginia Institutional Animal Care and Use Committee.

Surgery: V1. Mice were firstly anesthetized with isoflurane (5% for induction, 2% for maintenance, in O_2, ~0.5 L/min; VetFlo, Kent scientific). Once the animals lost reflexes, they were placed in a stereotaxic frame (Digital Model 1900, Stereotaxic Alignment System, Kopf Instruments) and the head was fixed by the ear bars as well as a tooth retainer. A plastic eye cover was placed above both eyes after applying

artificial tears (Henry Schein) to protect their vision during surgery. A rectal thermoprobe (Frederick Haer) was gently placed to detect the body temperature and a small heating pad was equipped with a feedback heater control module to modulate the heating level. The scalp was shaved to expose the skin. 70% ethanol and betadine were used to disinfect it. The skin was cut to expose the skull. The skull was cleaned with cotton swabs to remove connective tissue and scored by a razor blade to allow adherence later when adding the head plate.

A 2.5 mm in diameter craniotomy was performed 2.3 mm lateral from the midline and along the lambdoid suture in the left hemisphere of the skull using a dental drill and a 1⁄4 RA drill bit (Model XL-230, Osada, and Midwest Dental Equipment, respectively). A 2.5 mm circle was drilled, and the bone was lifted directly by a hook. Once the bone was removed, a piece of Gel foam (Pfizer Injectables) soaked with sterile saline solution was placed upon the exposed V1. AAV1-Syn-GCaMP6f viral vector (RRID: Addgene_100837; pAAV.Syn.GCaMP6f.WPRE.SV40, 1:1 in saline, titer2x-10^{13}) was injected using a Nanoject II (Drummond Scientific) fitted with a glass pipette with a beveled tip. The pipette was first filled with the mineral oil and loaded with the viral vector later. When the tip touched the V1 surface, the coordinate of the z-axis was set to zero. The pipette was lowered into V1 to 500 μm deep as the first injection depth and then retracted back to 250μm below the surface as the second injection depth. At each injection depth, a total volume of 23 nl was slowly delivered, in 10 pulses. Three sites were injected into each mouse across the latero-medial axis, 2.0 mm, 2.3 mm, and 2.6 mm from middle to lateral and near the lambdoid suture. The pipette was left in the brain tissue for 10 min before being slowly retracted so that the virus vector could be diffused completely.

Once injections were done, a three-layered glass window was placed over the craniotomy. The windows were made of 3 pieces of #1.5 glass coverslips, custom cut by Potomac Laser, glued together with UV glue (Norland Optical Adhesives). From top to bottom, they are a ring-shaped piece (inner diameter: 2.2 mm, outer diameter: 4.2 mm), and two disks (2.5 mm). Once the disk fit the craniotomy, windows were pushed down and sealed with VetBond (3M). A titanium headplate was mounted on the skull using Metabond (Parkell) mixed with black ink to avoid light reflections during imaging. An aluminum ring was glued on top of the head plate to hold water for immersion of the objective and block light from the surrounding environment. Mice were given a dose of carprofen (5 mg/Kg; Sub-Q) at the end of the surgery for pain and inflammation. A total amount of 0.1-0.5 ml of sterile saline (Sub-Q) was delivered during the surgery especially after bleeding. Once the Metabond was solid, animals were placed in a chamber with a heating pad until ambulatory and transferred back to their home cage. The surgery mice were monitored for at least four consecutive days for the pain and wound health. An additional dose of carprofen was given if the mice showed pain behaviors. Virus expression was checked using two-photon imaging 3 weeks after surgery.

Wide-field calcium imaging. For the V1 surgery mice, after fully recovering from surgery and the virus expressed well, their receptive field was confirmed with wide-filed imaging. A microscope (MVX10, Olympus) combing with a CCD camera (BU-61M, Bitran) was used to record calcium signals. The objective of the microscope was 0.63 ×, 0.15 NA objective (MV PLAPO, Olympus), and an Olympus U-M49002XL filter cube (excitation filter: 470/40 nm, dichroic mirror: 495 nm high pass, emission filter: 525/50 nm) was used. The exposed V1 surface under the glass window was excited with a 470 nm LED (UHP-T-LA, Prizmatix) of ~4.2 mW below the objective. Images were obtained in 240 × 135 pixels at 10 Hz with custom acquisition software (LabVIEW 2017, National Instrument). During recording, a monitor displaying Gabor gratings was moved to estimate the visual field of the contralateral eye of the imaging window. The mice were head-fixed and awake during imaging. Recorded images were used to determine the receptive field of the imaging window.

Surgery: SC. A similar procedure of V1 surgery was used for placing chronic cranial windows over SC (Savier et al., 2019). A 2.5 mm diameter craniotomy was performed over lambda. The skull was thinned until translucent and flexible. A piece of Gel foam soaked with sterile saline solution was placed upon the thinned skull to soften the remaining bone fragments. This helped to detach the bone fragments from the dura along the sutures. A hook was used to remove all the bone fragments. Gel foam soaked in saline was applied throughout the procedure which maintained osmosis of the exposed brain tissue and stopped bleeding. The dura was torn by a 30 G needle along the latero-medial axis and then along the rostrocaudal axis into two pieces. The caudal pole of the SC was revealed after lifting the two pieces of the dura. The SC windows were made of four pieces of glass coverslips, one ring, one disk, and two equilateral triangles (2 mm) from top to bottom. The tips of the triangle pieces allowed to catch the dura and push the transverse sinus anteriorly.

Two-photon calcium imaging. Before imaging, the mice were habituated to head fixation and running on the cylindrical treadmill for at least 3 days until they were comfortable. Imaging was performed under a two-photon scanning microscope (Ultima Investigator, Bruker Nano Surface Division; RRID: SCR_017142). A Ti: sapphire laser (Chameleon Discovery with TPC, Coherent) was used for imaging at an excitation wavelength of 920 nm for GCaMP6f using a 16 × 0.8 NA Nikon objective. Emitted signals were filtered into two PMTs (reference and response channels). The PrairieView software v5.4 was used to adjust the recording parameters and acquire imaging data. The parameters for recording were resonant scan in an acquisition rate of 30 Hz at 2× optical zoom, resulting in a 412.2 × 412.2 μm field-of-view. The image resolution was 512 × 512 pixels. 4-frame averaged data were used for the analysis. Imaging was performed in layer II/III of V1 (150-200 μm in depth) and sSGS of SC (no deeper than 50 μm from the SC surface). Note that animals that had sustained brain inflammation or had a poor expression of GCaMP6f were discarded from imaging.

Visual stimulus. Visual stimuli were delivered on an LCD monitor (59.7 × 33.6 cm, 60 Hz refresh rate, 50 cd/m2 mean luminance, gamma corrected). The screen could be moved and was placed 25 cm away from the animal's right eye which is the contralateral side of imaging. The exact location was adjusted with each recording according to the receptive field of imaged cells. V1 recording was done in the monocular region. The screen was centered between 60° and 90° across the azimuth (0° referring to the center of the binocular field) and between -10° and 0° in elevation (0° referring to eye level) reported in this study. For SC recording, the screen was centered between 90° and 120° across the azimuth and between 30° and 60° in elevation.

The visual stimulus was generated with the MATLAB Psychophysics toolbox (Brainard, 1997; Niell and Stryker, 2008; RRID: SCR_002881). The sinusoidal wave drifting gratings (100% contrast, 0.04 cpd, 2Hz for V1 and 0.08 cpd, 2 Hz for SC), or the plaids (adding two sinusoidal wave drifting gratings with a 90° or 120° across angle) are presented on gray background in a circular patch (60° diameter for V1; 40° diameter for SC) at the center of the screen. To assess direction selectivity, 12 different directions were tested, ranging from 0° to 330° in 30° intervals. A "blank" condition without showing anything was added to the 12 directions. Each stimulus condition was presented for 1 s, followed by a gray screen for 3 s, and shown at least 10 times randomly for every imaging. The timing and parameters of the visual stimulus were simultaneously recorded with the imaging data by the PrairieView software. The onset of the visual stimulus was synchronized with the onset of the calcium imaging and recorded in a third channel (in addition to the green channel for GCaMP6f and the red channel for tdTomato). Thirteen conditions were encoded in voltage signals in 7 inputs that could be analyzed after recording.

Imaging data analysis. We followed our published methods to analyze the 2-photon imaging data (Inayat et al., 2015; Barchini et al., 2018; Savier et al., 2019). In brief, every four time-series frames were

averaged to produce an image of the field-of-view to identify cells. When the imaging field shifted during recording caused by animals' movement, a pre-processing procedure written by MATLAB was used to realign the same cells. Regions of interest (ROIs) were manually drawn on the averaged image. The raw calcium signal was obtained from the averaged intensity of all pixels in each ROI. The fluorescence magnitudes or changes shown as $\Delta F/F_0$ was calculated by the $(F - F_0)/F_0$. F_0 was the baseline signal from the raw calcium signal that contain 6 frames before the stimulus. And F was the average 8 frames of fluorescence signals that 1 frame after the stimulus. If the $\Delta F/F_0$ was larger than 2 SD above the baseline signal for at least one condition, cells were considered as responsive to the stimulus.

Direction and orientation selectivity index. To quantify the degree of direction selectivity of each cell, we calculated a global direction selectivity index (gDSI), which is the vector sum of $\Delta F/F_0$ responses normalized by their scalar sum (Mazurek et al., 2014; Inayat et al. 2015; Shi et al. 2017; Savier et al. 2019):

$$gDSI = \frac{\sum R_\theta e^{i\theta}}{\sum R_\theta},$$

where R_θ is the response magnitude in $\Delta F/F_0$ at each direction of the stimulus.

We also calculated a global orientation/axis selectivity index (gOSI/gASI) to quantify the degree of preferred orientation or axis (bi-direction) selectivity:

$$gOSI/gASI = \frac{\sum R_\theta e^{i2\theta}}{\sum R_\theta}.$$

Note that we use gOSI and gASI interchangeably in this paper.

Partial correlation analysis. Cells having direction selectivity (gDSI > 0.2, SC) or axis selectivity (gASI > 0.2, V1) for the drifting gratings were selected to perform partial correlation analysis. This method was used in several studies, such as Gizzi et al. (1990), Smith et al. (2005), and Palagina et al. (2017), to calculate the motion selectivity of pattern and component. Based on the actual tuning curve obtained from the gratings, two predicted tuning curves were constructed to mimic either pattern or component tuning curve. The predicted pattern tuning curve is the same as the actual direction selective tuning curve. The hypothesized component tuning curve is changing the direction selective tuning curve to two peaks that are apart from the actual peak with half cross-angle of the plaids. For 90-degree plaids, the peaks shifted 45-degree to the left and right. Next, the formula was performed to calculate the partial correlation coefficients of component selective (R_c) and pattern selective (R_p).

$$R_c = (r_c - r_p r_{pc}) / \sqrt{(1 - r_p^2)(1 - r_{pc}^2)},$$

$$R_p = (r_p - r_c r_{pc}) / \sqrt{(1 - r_c^2)(1 - r_{pc}^2)},$$

where r_c is the linear Pearson correlation coefficient between the predicted tuning curve of component motion selectivity and the actual plaid tuning curve, r_p is the linear Pearson correlation coefficient between the predicted pattern motion tuning and the actual plaid tuning, and r_{pc} is the linear Pearson correlation between the predicted pattern and component motion tuning.

Finally, to calculate and visualize the cell numbers of selectivity for pattern or component motion, Fisher z-transform was used as in previous papers to calculate the associated z-scores:

$$Z_c = (\sqrt{(n-3)}) * 0.5 \ln * ((1+R_c) / (1-R_c)),$$

$$Z_p = (\sqrt{(n-3)}) * 0.5 \ln * ((1+R_p) / (1-R_p)),$$

where n is the number of different directions when performing drifting gratings (n=12 in our study). (n-3) is the number of degrees of freedom. To classify the component and pattern motion selective cells, we used 1.645 (95% confidence) as a criterion to measure the difference between Zp and Zc. A cell, if its (Z_c-Z_p) or Z_c itself was larger than 1.645, was considered as component motion selective. On the contrary, if a cell had (Z_p-Z_c) or Z_p larger than 1.645, was considered pattern motion selective. Otherwise, the cells were unclassified.

Pattern index. We also used a pattern index (PI) to scale the pattern motion selectivity to the component motion selectivity of each cell. The PI is calculated by subtracting the variance of the partial correlation coefficients of component selective (R_c) from the variance of the partial correlation coefficients of pattern selective (R_p) (Stoner & Albright, 1992; Pack et al., 2001; Guo et al.,2004).

$$PI = {R_p}^2 - {R_c}^2,$$

Positive values indicate cells are closer to the pattern motion selective, while negative values show the cells are more like component motion selective.

Results

V1 and SC neurons are tuned to different features of drifting gratings

We first tested the direction selectivity of V1 and SC cells using sinusoidal drifting gratings (see Materials and Methods). Once the GCaMP6f virus expressed well and the mice were comfortable with the cylindrical treadmill, two-photon calcium imaging was performed in Layer II/III of V1 or superficial layer of SC in awake mice (Fig. 1A). To ensure that the visual stimulus was placed in the correct place to stimulate the receptive fields of imaged cells, wide-field calcium imaging was used for V1 to locate the receptive field of the imaging window before 2 photon imaging (see Materials and Methods; Fig. 1E). Note that cells in the visual cortex show massive spontaneous activities. Therefore, the receptive field cannot be easily identified by our normal method for the SC (Inayat et al., 2015; Savier et al., 2019).

During two-photon calcium recording, we randomly displayed drifting gratings of 12 directions for at least 10 repeats in a circular patch (60° in diameter for V1 and 40° for SC). After recording, the calcium signal for individual neurons was processed and averaged for each direction. We applied statistical analysis according to the response magnitude to pick up responsive cells (see Materials and Methods) and eventually obtained 334 cells in V1 from 5 mice and 248 cells in SC from 6 mice. Interestingly, the tuning curves of responsive cells in each structure were clearly different. Most V1 cells showed two opposite peaks with narrow lobes, which means that they are bi-direction or motion axis selective. On the contrary, most SC cells presented only one wider lobe that was sensitive to a particular range of directions (Fig. 1B).

We calculated a global direction selectivity index and global orientation selectivity index (gDSI and gOSI; see Materials and Methods) for each cell for population analysis. We saw different distribution patterns between the two structures (Fig. 1C, D). V1 neurons showed high orientation selectivity, where the gOSI of most cells was higher than its gDSI (above the blue dashed line) and more than half of cells had their gOSI larger than 0.2, which is used conventionally as a cutoff of high selectivity. The data

points of SC neurons spread more areas of the plot and were higher in terms of direction selectivity. More SC cells had higher gDSI values than gOSI, especially in the gDSI ≥ 0.4 area, which is consistent with our previous reports of direction-selective cells in the very superficial layer of SC (Inayat et al., 2015).

V1 and SC neurons respond differently to plaids

Previous studies demonstrated two kinds of responses to plaids: pattern motion and component motion. The plaids were formed by superimposing two identical gratings at a certain cross angle. Pattern motion selective cells would respond to the global moving direction of the plaids and component motion selective cells would prefer the moving direction of elemental gratings of plaids (Fig.2A; red and blue arrows). In our study, we used plaids with a 90-degree cross angle. For V1, the drifting plaids were formed using sinusoidal gratings of 100% contrast, 0.04 cpd, 2Hz in a 60-degree circular patch (Fig.2A), whereas, for the SC, the elemental gratings were 0.08 cpd in a 40-degree circular patch. We selected the parameters based on the preference of each area according to previous studies (refs).

To test component or pattern motion selectivity, we firstly selected direction/ bi-direction selective cells from each area. The responses in V1 were generally lower than in SC. Therefore, we used the criteria of maximal response amplitudes ($\Delta F/F_0$) larger than 10% (vs. 20% for SC) and gASI larger than 0.2. This resulted in 101 bi-direction selective V1 cells (from 334 grating responsive cells, 30.42%). Next, we calculated the maximal response amplitude, gDSI, preferred direction, and gOSI of each cell to gratings and plaids. The maximal responses to plaids were not correlated with those to gratings in V1 (Fig. 2B; top). For example, several cells that responded strongly to plaids were weakly responsive to gratings. Also, most cells in V1 had low gDSI to both stimuli (Fig. 2C; top). The preferred directions to gratings and plaids were different too (Fig. 2D; top). Interestingly, the majority of bi-directional selective cells to gratings had their gOSI lower than 0.2 to plaids. In other words, they were not axis selective anymore (Fig. 2E; top).

For the SC, 141 cells (from 248 grating responsive cells, 56.85%) had maximal response amplitudes larger than 20% and gDSI larger than 0.2. In strong contrast to V1, these SC neurons showed similar responses to plaids as to gratings. The maximal response amplitudes of SC neurons to plaids were consistent with gratings but slightly stronger (Fig. 2B; bottom). Furthermore, the preferred direction was similar between gratings and plaids (along the diagonal dash line; Fig. 2C, D; bottom), whereas the direction selectivity (gDSI) to plaids was weaker than to gratings.

These results suggest that most SC neurons prefer the same motion direction of plaids to gratings, which are the global motion direction of plaids. They are pattern motion selective cells. However, V1 neuron responses to plaids were not tuned to the global motion.

V1 neurons appear component motion selectivity and are predominantly unclassified

Due to the complicated results from population plots, we investigated the tuning curves of individual cells to plaids for a better understanding. Surprisingly, we found that V1 cells responded to plaids in various ways (Fig. 3B, C). Some neurons (four examples in Fig. 3C), such as the first cell preferred 345-degree motion direction to plaids but was not responsive to gratings. Another group of V1 neurons was selective to component motion (Fig. 3A, B). Such cells responded to gratings in axis directions (Fig. 3A; left) and were selective to the motion directions of elemental gratings. They showed a four-peak tuning curve and approximately 90-degree away from each other to plaids (Fig. 3A; right). Also, a large proportion of V1 cells responded to gratings but not to plaids.

To quantify the proportion of the component cells, the partial correlation coefficients were calculated between the predicted tuning and actual tuning of each cell (see Materials and Methods). Among the 101 axis motion selective cells, we found that a bit more cells (59 cells; 58.42%) have higher Rc than Rp (Fig. 3D; below the diagonal dash line). The z-score space derived from the partial correlation reveals that 12 component selective cells (from 101 bi-direction selective cells; 11.88%) were identified and only 3 were classified as pattern motion selective cells (2.97%). A large number of cells (85.15%) were unclassified (Fig. 3E). The distribution of Pattern index versus gOSI again supports our finding that slightly more component-trending cells (53 cells; 52.48%) than pattern-tending cells in the bi-direction cells of V1, especially for the high axis motion selective cells (Fig. 3G; cells with negative values).

Furthermore, the pattern motion selective cells identified by the partial correlation coefficients might not be truly pattern motion selective, but weakly responsive to plaids (Fig. 3F; left). The tuning curves of unclassified cells were mostly flat which indicates those cells were not sensitive to specific motion directions (Fig. 3F; middle). Together, our results suggest that V1 neurons process complex motion in several ways and do not always fall into simple categories of pattern motion vs component motion.

SC neurons show robust pattern motion selectivity

As described above, SC neurons are different from V1 neurons in responding to plaids (Fig. 2B, C, D, E). When investigating tuning curves of individual cells, SC responses to plaids (Fig. 4A; red) were similar to gratings (Fig. 4A; blue), including the shape of the tuning curve and preferred directions (Fig. 4A, B). Again, it illustrates that SC neurons are predominantly pattern motion selective. Moreover, many SC neurons responded more strongly to plaids but were less direction selective than gratings, as reflected by the red curves being higher and broader than blue curves, as seen from the population level (Fig. 2B, C; bottom).

Same as V1, the partial correlation coefficient and z-score space were used to identify the proportion of pattern cells. About 83.69% (118/141) of cells were correlated more with pattern motion selective (Fig. 4C; above the blue dash line). 81 cells (57.45% of direction-selective cells) were identified as pattern motion selective, while only 5 cells (3.55%) as component motion selective and 55 cells (39.01%) as unclassified (Fig. 4D). The distribution of Pattern index versus gDSI presented the similar result that 86.52% cells (122/141) were pattern-trending motion selective (Fig. 4F; cells with positive values). In addition, the component motion selective cells identified by this method responded very weakly or broadly to plaids (Fig. 4E; right). Similar results showed in unclassified cells as well (Fig. 4E; middle). Therefore, our results indicate that component cells are a very small minority in the superficial SC.

Discussion

Mouse layer II/III V1 and superficial SC are differently sensitive to sinusoidal drifting gratings

In response to sinusoidal drifting gratings, the superficial layer of SC neurons was mostly selective for motion direction (DS), whereas layer II/III of V1 was mostly bi-direction selective cells. The difference is consistent with previous reports (Inayat et al., 2015; Savier et al., 2019) and indicates that V1 and SC process motion in different ways. DS cells in the SC may simply be sensitive to an estimated moving direction of objects that facilitate the animal to avoid their predators and respond faster in danger. As part of the cortex, V1 cells may respond to more details of the visual stimulation and have more complex functional organization.

In addition, the SC cells' tuning curves were broader than V1 cells. The broader tuning curve again suggested that SC cells were roughly responsible for a range of directions. But V1 cells preferred precise directions or motion axis. This provides possibilities for V1 to accurately process complex motion.

Mouse V1 and SC are differently sensitive to symmetrical plaids

We used 90-degree cross-angle plaids to test the selectivity for either pattern or component motion. Interestingly, we found that some V1 cells were component motion selective while most SC direction-selective cells were pattern motion selective. On the other hand, the response magnitudes of SC cells to plaids were as high as to gratings. The tuning curves to plaids also had similar shapes with that to gratings. These findings suggest that SC cells treat gratings and plaids similarly. In other words, the visual information of plaids and gratings captured by these SC neurons is similar. On the contrary, V1 cells responded to gratings and plaids significantly differently, in terms of tuning curve and response magnitude. This indicates that V1 could identify those gratings and plaids as two different stimuli, also suggesting that V1 may encode more details of motion information.

Our study is the first to study the plaid motion selectivity in the visual cortex of awake mice. Compared with the three recent papers that used plaids in anesthetized mouse V1 (Juavinett & Callaway, 2015; Muir et al., 2015; Palagina et al., 2017), our results support Juavinett and Callaway's study that no pattern cells were found in layer II/III. Only three pattern cells were identified by the partial correlation quantification in our study, but it turned out that their responses were rather weak. A number of V1 cells, which were either not responsive or selective to gratings, did respond to a preferred direction of plaids.

Mouse V1 and SC show similar properties to complex motion with higher mammals

Moving plaids have been used for a long time to test the global and local motion selectivity. Previous studies were mostly done in primates and cats using electrophysiology. With the development of new technology, a recent study has been done in primates by two-photon calcium imaging like our study (Guan et al. 2020). Interestingly, their findings have many in common with our mouse study. For instance, both studies found that many weak or non-orientation-tuned neurons in V1 are strongly responsive to plaids (Fig. 2B,3F). Furthermore, they showed that most orientation-tuned V1 neurons have cross-orientation inhibition to plaids. Our results also showed the majority orientation tuned V1 neurons respond much weaker to plaids and were not orientation selective anymore (Fig. 2B, E). One recent study shows that this cross-orientation interaction in mice is caused by feedforward mechanisms (Barbera et al., 2022), which may not be the case in the SC.

Little has been done to examine the pattern and component motion selectivity by plaids in the SC, but one study used random line patterns to test the direction-tuning property of SC in cats (Zhao et al., 2005). The random line stimuli are composed of identical short lines moving in a direction that has an angle with the orientation of these short lines. Therefore, it can test the pattern (sensitive to veridical moving direction) or component (sensitive to the moving direction of component lines) motion selectivity in single cells. About 50% of SC cells mostly from the superficial layer were found to be pattern motion selective when the lines are short (L=1 degree) and 25% when lines are longer (L=3 degree). We showed a similar result that more than half of the direction-tuning cells were pattern motion selective. Due to the stimulus and species differences, the exact proportion of the pattern cells is hard to compare. But both our studies at least demonstrated that pattern motion selective cells exist in the SC.

Both our studies have limitations in that we only investigated the superficial layer of SC. It is possible that component cells exist in deeper layers since they oversee the sensorimotor transformation. Moreover, even though most of the studies used the same partial correlation coefficient to quantify the cell numbers

of component and pattern motion, better quantification methods may still be needed in the future which could take the consideration of weak or broad responses.

Non-component motion selective cells in V1 could still contribute to complex motion processing

A large proportion of V1 cells responded to either gratings or plaids but not to both (Fig. 2B). Such cells could contribute to motion integration at the population level since they are sensitive to one of the moving stimuli. Furthermore, a previous paper reported that V1 neurons respond differently to plaids that have different cross-angle (Palagina et al., 2017). Along with other examples, the study concluded that pattern-motion and component-motion selectivity were highly dependent on the cross angle. This finding again suggests that V1 cells deal with the details of complex motion signals.

On the contrary, pattern motion selective cells in SC are very consistent. We also tested the cross-angle of 120-degree plaids in SC and found that they are also mostly pattern motion selective (data not shown). Their preferred directions of plaids were even more consistent with gratings than 90-degree plaids, which makes sense since our grating stimuli were 12 directions with 30 degrees apart. As a result, 120-degree plaids have a global direction that's directly tested with gratings (60 degrees from the two gratings vs 45 degrees in the case of 90-degree plaids). On the other hand, for component cells, 90 degrees is narrower than 120 degrees, and may be harder to differentiate the two peaks in the tuning curves, especially for SC cells where the tuning curves are normally broad. This result also indicates that 120-degree plaids are better than 90-degree plaids when testing both pattern and component motion selectivity for DS cells. However, for V1 cells that are tuned to two directions of the same motion axis, 90-degree plaids are better than 120-degree ones to maximize the separation of the tuning curve peaks.

Conclusion

We tested the complex motion selectivity of mouse Superior Colliculus and Primary Visual Cortex by using two-photon calcium imaging and found a significant difference between the two structures. We showed that SC neurons were primarily pattern-sensitive, meaning that they responded preferentially to the global motion direction of the plaid stimuli. In contrast, very few V1 neurons were pattern motion selective, and some were in fact component motion selective. Our data show a difference in how V1 and SC compute complex motion signals via LGN transformation or directly from the retina, respectively.

Acknowledgment

I am extremely grateful to my advisor Prof. Cang. I couldn't finish this project and the predissertation paper without his guidance and advice. I am also thankful for Victor's contribution to SC data collection and editing of the method part of this predissertation paper. I sincerely appreciate that he taught me how to use 2 photon imaging and analysis the data when I started my first year in the lab. Thanks also should go to Prof. Meliza that who serves as the second reader of my predissertation paper.

References

Adelson, E. H., & Movshon, J. A. (1982). Phenomenal coherence of moving visual patterns. *Nature*, *300*(5892), 523-525.

Albright, T. D., & Stoner, G. R. (1995). Visual motion perception. *Proceedings of the National Academy of Sciences*, *92*(7), 2433-2440.

Barbera, D., Priebe, N. J., & Glickfeld, L. L. (2022). Feedforward mechanisms of cross-orientation interactions in mouse V1. *Neuron*, *110*(2), 297-311.

Bonin, V., Histed, M. H., Yurgenson, S., & Reid, R. C. (2011). Local diversity and fine-scale organization of receptive fields in mouse visual cortex. *Journal of Neuroscience*, *31*(50), 18506-18521.

Cang, J., Savier, E., Barchini, J., & Liu, X. (2018). Visual function, organization, and development of the mouse superior colliculus. *Annu Rev Vis Sci*, *4*, 239-262.

Dhande, O. S., & Huberman, A. D. (2014). Retinal ganglion cell maps in the brain: implications for visual processing. *Current opinion in neurobiology*, *24*, 133-142.

Ellis, E. M., Gauvain, G., Sivyer, B., & Murphy, G. J. (2016). Shared and distinct retinal input to the mouse superior colliculus and dorsal lateral geniculate nucleus. *Journal of neurophysiology*, *116*(2), 602-610.

Gizzi, M. S., Katz, E., Schumer, R. A., & Movshon, J. A. (1990). Selectivity for orientation and direction of motion of single neurons in cat striate and extrastriate visual cortex. *Journal of neurophysiology*, *63*(6), 1529-1543.

Guan, S. C., Zhang, S. H., Zhang, Y. C., Tang, S. M., & Yu, C. (2020). Plaid detectors in macaque V1 revealed by two-photon calcium imaging. *Current Biology*, *30*(5), 934-940.

Guo, K., Benson, P. J., & Blakemore, C. (2004). Pattern motion is present in V1 of awake but not anaesthetized monkeys. *European Journal of Neuroscience*, *19*(4), 1055-1066.

Hildreth, E. C., & Koch, C. (1987). The analysis of visual motion: From computational theory to neuronal mechanisms. *Annual review of neuroscience*, *10*, 477-533.

Hübener, M. (2003). Mouse visual cortex. *Current opinion in neurobiology*, *13*(4), 413-420.

Inayat, S., Barchini, J., Chen, H., Feng, L., Liu, X., & Cang, J. (2015). Neurons in the most superficial lamina of the mouse superior colliculus are highly selective for stimulus direction. *Journal of Neuroscience*, *35*(20), 7992-8003.

Juavinett, A. L., & Callaway, E. M. (2015). Pattern and component motion responses in mouse visual cortical areas. *Current Biology*, *25*(13), 1759-1764.

Khawaja, F. A., Tsui, J. M., & Pack, C. C. (2009). Pattern motion selectivity of spiking outputs and local field potentials in macaque visual cortex. *Journal of Neuroscience*, *29*(43), 13702-13709.

Mazurek, M., Kager, M., & Van Hooser, S. D. (2014). Robust quantification of orientation selectivity and direction selectivity. *Frontiers in neural circuits*, *8*, 92.

Movshon JA, Adelson EH, Gizzi MS, Newsome WT (1985) The analysis of moving visual patterns. In: Study week on pattern recognition mechanisms (Chagas C, Gattass R, Gross C, eds), pp 117–151. Rome, Italy: Vatican.

Muir, D. R., Roth, M. M., Helmchen, F., & Kampa, B. M. (2015). Model-based analysis of pattern motion processing in mouse primary visual cortex. *Frontiers in neural circuits*, *9*, 38.

Ohki, K., Chung, S., Ch'ng, Y. H., Kara, P., & Reid, R. C. (2005). Functional imaging with cellular resolution reveals precise micro-architecture in visual cortex. *Nature*, *433*(7026), 597-603.

Ohki, K., & Reid, R. C. (2007). Specificity and randomness in the visual cortex. *Current opinion in neurobiology*, *17*(4), 401-407.

Pack, C.C., Berezovskii, V.K. & Born, R.T. (2001) Dynamic properties of neurons in cortical area MT in alert and anaesthetized macaque monkeys. *Nature*, 414, 905–908.

Palagina, G., Meyer, J. F., & Smirnakis, S. M. (2017). Complex visual motion representation in mouse area V1. *Journal of Neuroscience*, *37*(1), 164-183.

Rodman, H. R., & Albright, T. D. (1989). Single-unit analysis of pattern-motion selective properties in the middle temporal visual area (MT). *Experimental Brain Research*, *75*(1), 53-64.

Savier, E. L., Chen, H., & Cang, J. (2019). Effects of locomotion on visual responses in the mouse superior colliculus. *Journal of Neuroscience*, *39*(47), 9360-9368.

Shi, X., Barchini, J., Ledesma, H. A., Koren, D., Jin, Y., Liu, X., ... & Cang, J. (2017). Retinal origin of direction selectivity in the superior colliculus. *Nature neuroscience*, *20*(4), 550-558.

Smith, M. A., Majaj, N. J., & Movshon, J. A. (2005). Dynamics of motion signaling by neurons in macaque area MT. *Nature neuroscience*, *8*(2), 220-228.

Stoner, G.R. & Albright, T.D. (1992) Neural correlates of perceptual motion coherence. *Nature*, 358, 412–414.

Wang, L., Sarnaik, R., Rangarajan, K., Liu, X., & Cang, J. (2010). Visual receptive field properties of neurons in the superficial superior colliculus of the mouse. *Journal of Neuroscience*, *30*(49), 16573-16584.

Zhao, B., Chen, H., & Li, B. (2005). Pattern motion and component motion sensitivity in cat superior colliculus. *Neuroreport*, *16*(7), 721-726.

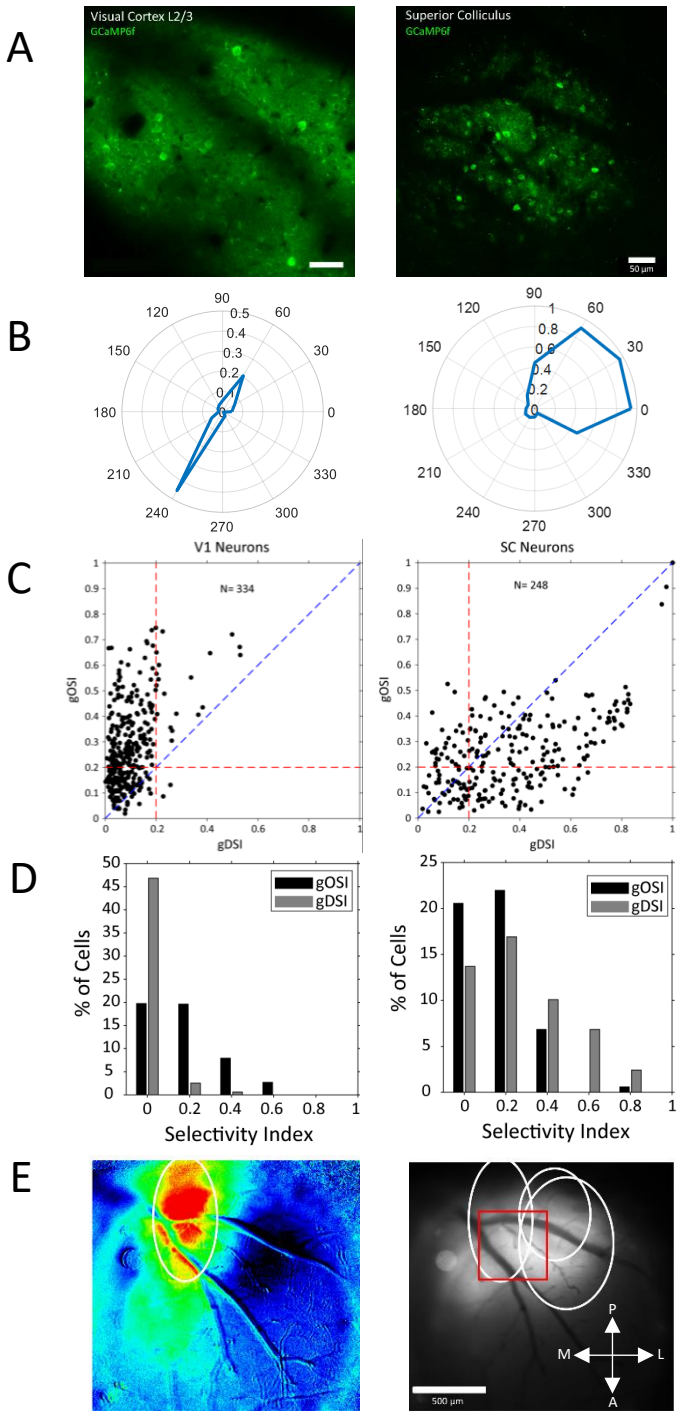

Figure 1. V1 and SC neurons are tuned to different features of drifting gratings. **A**, Two-photon imaging of layer II/III V1 (left) and the superficial layer of the SC (right). Green, GCaMP6f expressing cells. **B,** Example cells of V1 (left) and SC (right) tuned to drifting gratings. **C, D,** Comparison of neurons' responses to drifting gratings between V1 (n=334 neurons from 5 mice) and SC (n=248 neurons from 6 mice). **E,** Retinotopic map of V1 by wide-field GCaMP imaging. Left, response heat map at 90° azimuth, 0° elevation. Right, White circles (left to right) represent receptive fields of 90° azimuth, 0° elevation; 45° azimuth, 0° elevation; 45° azimuth, -10° elevation. Red square is roughly the area imaged under the Two-photon microscope.

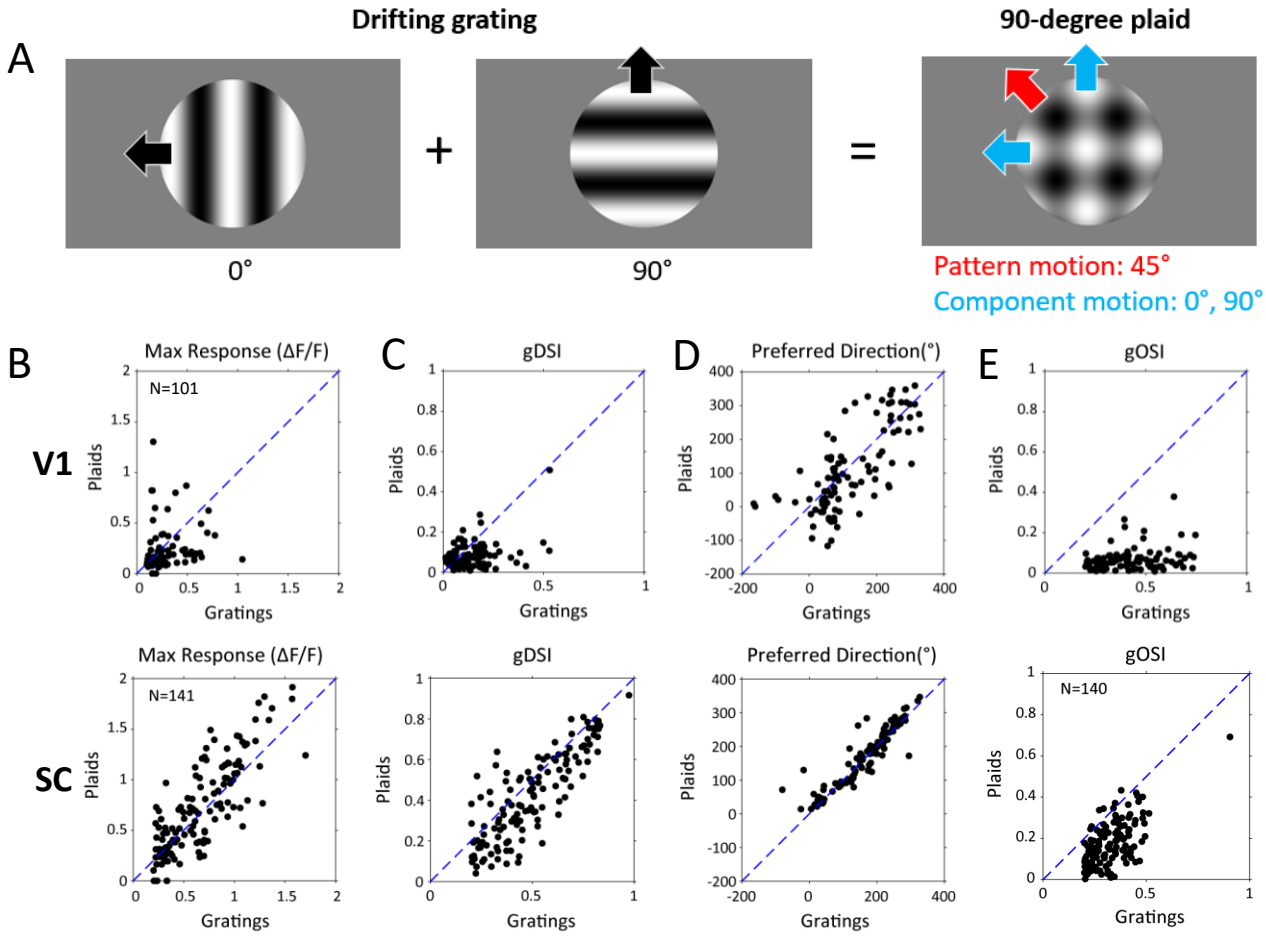

Figure 2. V1 and SC neurons respond differently to plaids. **A,** Schematic of visual stimuli: sinusoidal drifting grating and plaid of 90° cross angle. **B,C,D,E,** Comparison of the maximal response amplitude, gDSI, preferred direction, and gOSI to drifting gratings vs plaids between V1 cells (n=101 neurons from 5 mice; ΔF/F>0.1, gOSI>0.2) and SC cells (n=141 neurons from 6 mice; ΔF/F>0.2, gDSI>0.2).

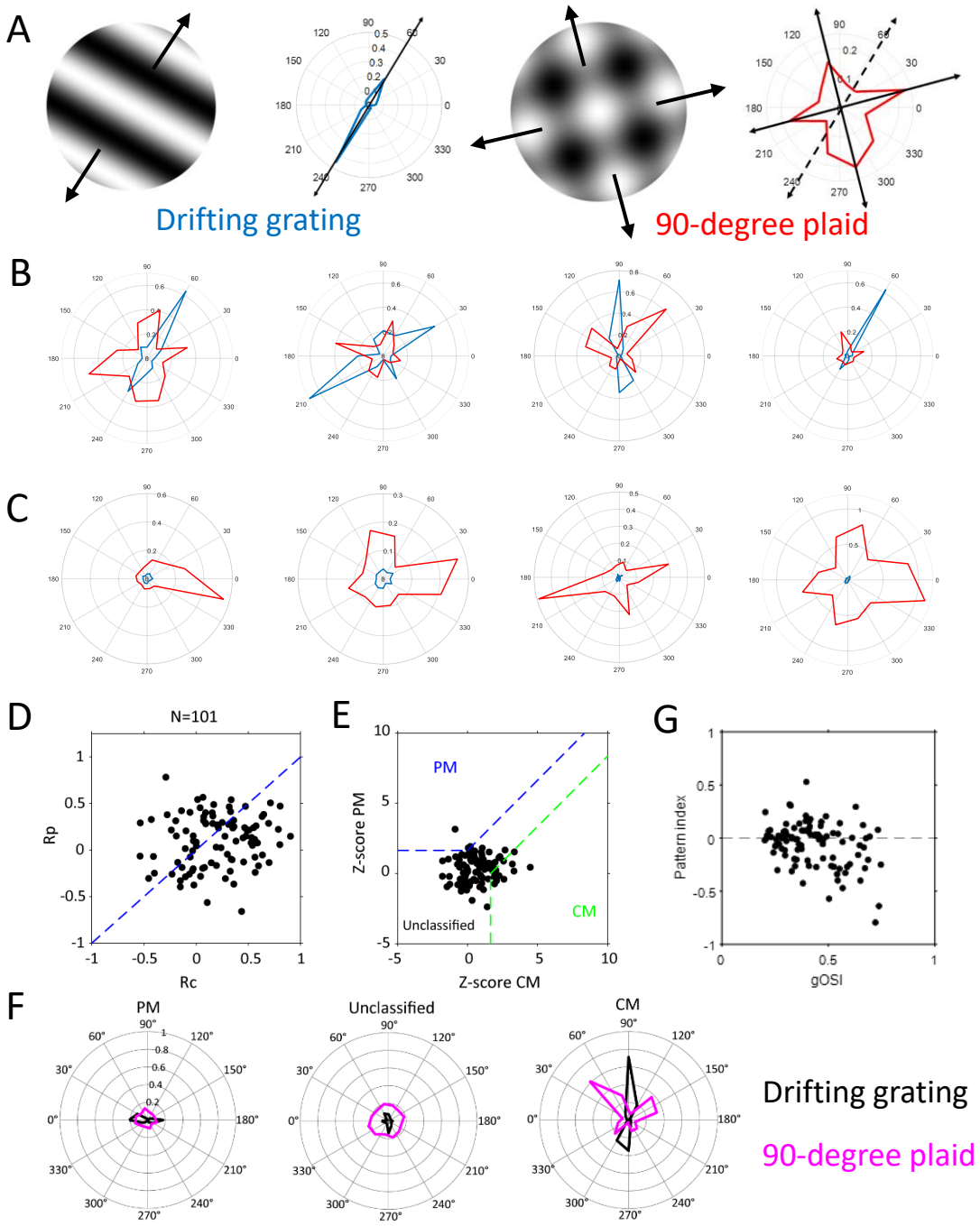

Figure 3. V1 neurons' responses to plaids. **A,** An example cell of component motion selective in V1 showing by polar plot and its schematic visual stimuli. **B,** More example cells. **C**, Examples of plaid-preferred cells. **D,** The partial correlation coefficients (PM-selective response (R_p) and CM-selective response (R_c)) of V1 cells by adjusting for the correlation between predictions. **E,** The Fisher z-transform to calculate the associated z-scores to rate the selectivity for pattern versus component motion of each cell. PM = 3, Uncl = 86, CM = 12. **F,** Examples of pattern motion, unclassified, and component motion selective cells. **G,** Pattern index vs gOSI of V1 cells. Positive pattern index indicates larger R_p.

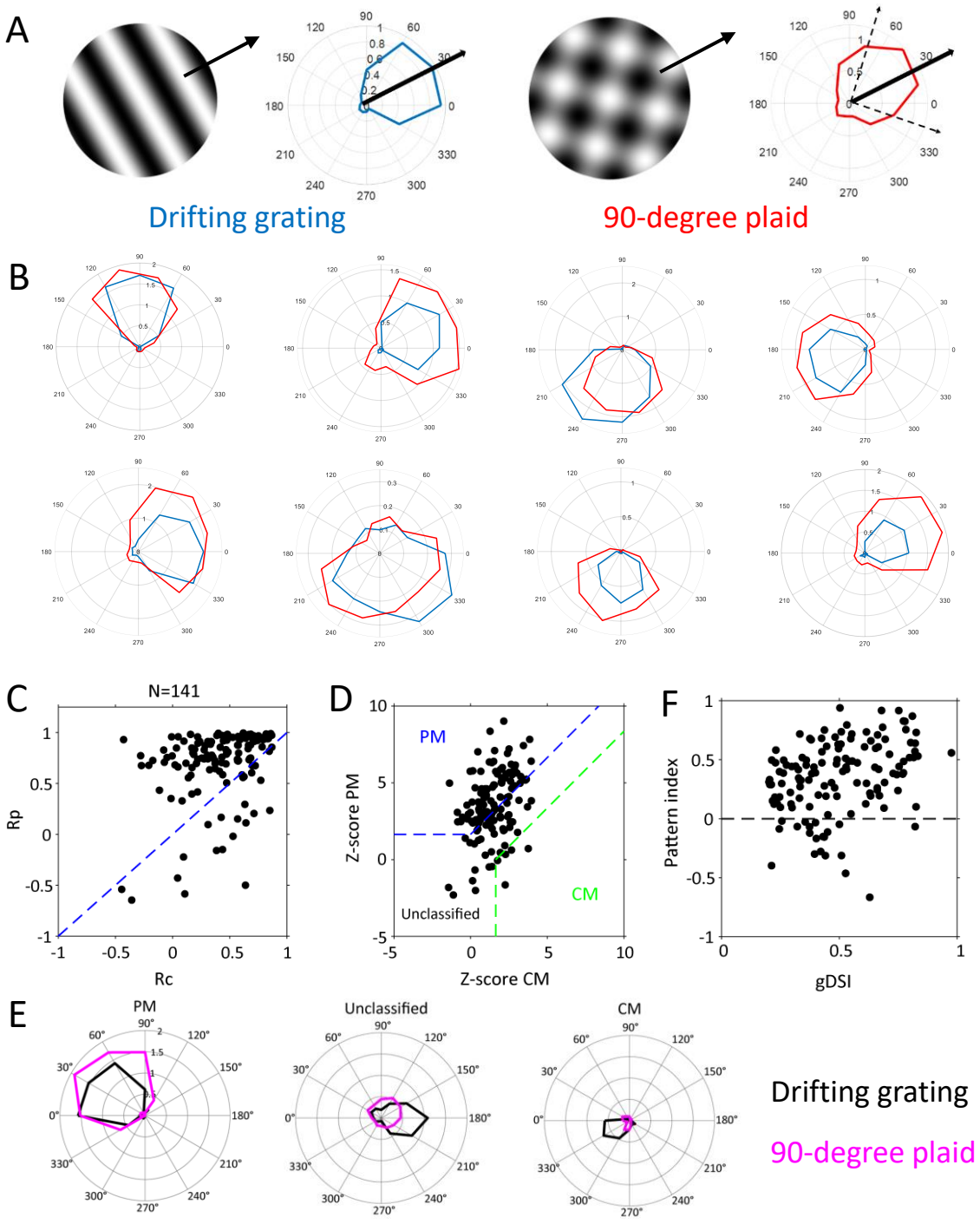

Figure 4. SC neurons show robust pattern motion selectivity. **A,** An example cell of pattern motion selective in SC showing by polar plot and its schematic visual stimuli. **B,** More example cells. **C,** The partial correlation coefficients (PM-selective response (R_p) and CM-selective response (R_c)) of SC cells by adjusting for the correlation between predictions. **D,** The Fisher z-transform to calculate the associated z-scores to rate the selectivity for pattern versus component motion of each cell. PM = 81, Uncl = 55, CM = 5. **E,** Examples of pattern motion, unclassified, and component motion selective cells. **F,** Pattern index vs gOSI of SC cells. Positive pattern index indicates larger R_p.